

Dark matter and Modified Newtonian Dynamics in a sample of high-redshift galaxy clusters observed with Chandra

Carl Blaksley^a, Massimiliano Bonamente^b

^a*Department of Physics, University of Alabama, Huntsville, AL, USA and
Arnold Sommerfeld Center For Theoretical Physics, Faculty of Physics,
Ludwig-Maximilians Universität, München, Germany*

^b*Department of Physics, University of Alabama, Huntsville, AL, USA and
NASA National Space and Science Technology Center, Huntsville, AL, USA*

Abstract

We compare the measurement of the gravitational mass of 38 high-redshift galaxy clusters observed by *Chandra* using Modified Newtonian Dynamics (MOND) and standard Newtonian gravity. Our analysis confirms earlier findings that MOND cannot explain the difference between the baryonic mass and the total mass inferred from the assumption of hydrostatic equilibrium. We also find that the baryon fraction at r_{2500} using MOND is consistent with the Wilkinson Microwave Anisotropy Probe (WMAP) value of Ω_B/Ω_M .

Key words: galaxies: clusters: general
cosmology: dark matter
95.35.+d
95.85.Nv

1. Introduction

Since the introduction by Milgrom in 1983 (Milgrom, 1983), MOND had success in explaining galaxy rotation curves using only the mass-to-light ratio as a free parameter, and was able to predict the applicability of the Tully-Fisher relation to low surface brightness galaxies before dynamic information on them was available (Scarpa, 2006). These successes are not surprising, given the fact that MOND was created as a phenomenological theory in order to eliminate the need for dark matter in galaxies.

While there have been numerous applications of MOND to individual galaxies, it is also important to study MOND on those scales where dark

matter is believed to dominate, in particular that of galaxy clusters. There have been far fewer studies of MOND on this scale, with previous work on the subject including Sanders (1999), Aguirre et al. (2001), Pointecouteau & Silk (2005) and Angus et al. (2008). These results indicate that MOND does not eliminate the need for dark matter in galaxy clusters. In this paper we use MOND to calculate gravitational and baryonic masses for a sample of 38 galaxy clusters. The motivation of this work is the need to confirm the previous results by using a larger sample of massive clusters at high redshift ($z=0.14-0.89$).

We begin with a brief overview of the data and the models used, found in Section 2. Section 3 describes the calculation of the gas mass using X-ray observation, the derivation of the MOND acceleration, and the calculation of total masses from hydrostatic equilibrium. We then present our results in Section 4 and our conclusions in Section 5. The cosmological parameters $h = 0.7$, $\Omega_M=0.3$ and $\Omega_\Lambda=0.7$ are used throughout this work.

2. Chandra X-ray Data And Data Modeling

We analyze *Chandra* X-ray data from 38 clusters in the redshift range $z=0.14-0.89$ (Table 1). The *Chandra* observations and the data modeling with the isothermal β model are presented in Bonamente et al. (2006); LaRoque et al. (2006); Bonamente et al. (2008). Here those aspects of the data modeling and analysis that are relevant to the present investigation.

The electron density model is based on the isothermal spherical β -model (Cavaliere & Fusco-Femiano, 1976, 1978), which has the form

$$n_e(r) = n_{e0} \left(1 + \frac{r^2}{r_c^2} \right)^{-3\beta/2}, \quad (1)$$

where n_{e0} is the central electron number density, r_c is a core radius, and β is a power-law index. The radial profile of the X-ray surface brightness is obtained via integration along the line of sight, and results in the following analytical expression:

$$S_x = S_{x0} \left(1 + \frac{\theta^2}{\theta_c^2} \right)^{(1-6\beta)/2}. \quad (2)$$

Best-fit model parameters and confidence intervals for all model parameters are obtained using a Markov chain Monte Carlo (MCMC) method described in detail by Bonamente et al. (2004) and LaRoque et al. (2006). For each cluster, the Markov chain constrains the parameters S_{x0} , β , θ_c ,

T_e , and the chemical abundance (see LaRoque et al. 2006 for best-fit values). We use the cosmological parameters $h = 0.7$, $\Omega_M=0.3$ and $\Omega_\Lambda=0.7$ to calculate each cluster's angular diameter distance D_A (e.g., Carroll et al., 1992).

All of our calculations are done out to a maximum radius of r_{2500} , the radius at which the cluster mass density is 2500 times the critical density, which is also approximately the radius out to which our *Chandra* data are sensitive without any extrapolation of the models. In LaRoque et al. (2006) we have compared masses obtained using the simple isothermal β model with those obtained using a more complex non-isothermal β model, and shown that the two methods yield the same ratio of baryonic to total mass. The non-isothermal model included a double β model distribution for the density (Equation 7 in LaRoque et al. 2006), and an arbitrary temperature profile that was constrained by assuming that the plasma is in hydrostatic equilibrium with an NFW potential (Equation 8 in LaRoque et al. 2006). We therefore expect no significant bias in the study of MOND masses using this simple model, which has the advantage of analytical expressions for the observables and the masses.

3. Calculation of gas, Newtonian and MOND Masses

For the isothermal β model, the gas mass enclosed within a given cluster radius is given by (e.g. LaRoque et al., 2006)

$$M_{gas}(r) = A \int_0^{r/D_A} \left(1 + \frac{\theta^2}{\theta_c^2}\right)^{-3\beta/2} \theta^2 d\theta, \quad (3)$$

where $A = 4\pi\mu_e n_{e_o} m_p D_A^3$, μ_e is the mean electron weight (calculated from the *Chandra* data, with typical value of $\mu_e = 1.17$), and D_A is the cluster distance. The central electron density n_{e_o} is calculated from the X-ray surface brightness (LaRoque et al., 2006; Birkinshaw et al., 1991) as

$$n_{e_o} = \left[\frac{S_{x_o} 4\pi(1+z)^4 (\mu_H/\mu_e) \Gamma(3\beta)}{\Lambda_{eH} D_A \pi^{1/2} (3\beta - 1/2) \theta_c} \right]^{1/2}, \quad (4)$$

in which μ_H is the mean hydrogen weight (typical value $\mu_H = 1.4$), and Λ_{eH} is the emissivity of the plasma. The gas mass in Equation (3) is measured directly from observables and does not depend on the law of gravity in any way.

For the total mass, M_{total} , we solve the hydrostatic equilibrium equation using Newtonian gravitation and the ideal gas law, to obtain the Newtonian mass:

$$M_{total}(r) = -\frac{kr^2}{Gn_e(r)\mu_{tot}m_p} \left[T_e(r) \frac{dn_e(r)}{dr} + n_e(r) \frac{dT_e(r)}{dr} \right], \quad (5)$$

in which μ_{tot} is the mean molecular weight (typical value $\mu_{tot} = 0.61$). Owing to our use of an isothermal model, the second term goes to zero and using Equation (1) it becomes

$$M_{total}(r) = \frac{3\beta kT_e}{G\mu m_p} \frac{r^3}{r_c^2 + r^2}. \quad (6)$$

Starting with the most basic form of MOND (Pointecouteau & Silk, 2005; Scarpa, 2006), we derive the gravitational mass based on the MOND law of gravity. The MOND acceleration (a) is related to the Newtonian acceleration (a_N) by the relation

$$\frac{GM(r)}{r^2} = a_N = a \cdot \mu\left(\frac{a}{a_o}\right). \quad (7)$$

where a_o is a critical acceleration that is meant to be a new physical constant and represents the acceleration below which Newtonian gravity is no longer valid (Milgrom, 1983; Scarpa, 2006); the function μ is any interpolating function that provides a transition between the two regimes. We take the critical acceleration to be $a_0 = 1.17e^{-8} \text{ cm/s}^2$ as used in Angus et al. (2008); this value is derived from galaxy rotation curve fits Scarpa (2006). In Section 4 we also discuss the results obtained using a variable value of the critical acceleration.

The interpolating function $\mu(x)$ is any function which yields the appropriate asymptotic behavior,

$$\mu(x) = \begin{cases} 1 & \text{for } x \gg 1 \\ x & \text{for } x \ll 1 \end{cases}$$

The most used interpolating function (Scarpa, 2006; Pointecouteau & Silk, 2005), and the one which we use here, is

$$\mu(x) = \frac{x}{\sqrt{1+x^2}}. \quad (8)$$

Using Equation (8) in Equation (7) and solving for a , gives us the relation

$$a^2 = a_N^2 \left(\frac{1}{2} + \frac{1}{2} \sqrt{1 + \frac{4a_\circ^2}{a_N^2}} \right). \quad (9)$$

Equation (9) is the MOND acceleration as a function of the Newtonian acceleration and the critical acceleration parameter (see also Pointecouteau & Silk, 2005). We use the hydrostatic equilibrium equation according to MOND,

$$-\frac{1}{\rho_g(r)} \frac{dP_g}{dr} = a(r), \quad (10)$$

($\rho_g(r)$ is the gas density and P_g its pressure) in order to determine the MOND equation for total mass analogous to Equation (6) for Newtonian gravity. Using Equations (9) and (10) with $a_N = GM(r)/r^2$ leads to the elimination of the Newtonian acceleration a_N :

$$\frac{GM(r)}{r^2} = \frac{\left(\frac{-1}{\rho(r)} \frac{dP}{dr} \right)^2}{\sqrt{\left(a_\circ^2 + \left(\frac{-1}{\rho(r)} \frac{dP}{dr} \right)^2 \right)}}. \quad (11)$$

For the β model profile of density we obtain:

$$M_{MOND}(r) = \frac{\frac{r^2}{G} \left(\frac{3\beta KT}{\mu m_p} \frac{r}{r_c^2 + r^2} \right)}{\sqrt{a_\circ^2 + \left(\frac{3\beta KT}{\mu m_p} \frac{r}{r_c^2 + r^2} \right)^2}}. \quad (12)$$

This equation can be further simplified when one realizes that the numerator is the total mass according to Newtonian dynamics, Equation (6). This simplification gives us a final equation for the total mass based on the hydrostatic equilibrium condition and using MOND gravity.

$$M_{MOND}(r) = \frac{M_{Newton}(r)}{\sqrt{1 + \left(\frac{a_\circ \mu m_p}{3\beta KT} \frac{(r_c^2 + r^2)}{r} \right)^2}} \quad (13)$$

This equation displays the appropriate asymptotic behavior, namely that for a critical acceleration of zero we recover the Newtonian M_{total} .

4. Results

4.1. Comparison of Newtonian and MOND gravitational masses

Having found an equation for the MOND total mass (M_{MOND}) we calculate M_{gas} , M_{total} and M_{MOND} for each of the 38 galaxy clusters in our sample out to a radius of r_{2500} . In each case M_{gas} was calculated using Equation (3), M_{total} by means of Equation (6), and M_{MOND} using Equation (13). For each cluster, the MOND gravitational mass is lower than the the Newtonian gravitational mass by just $\sim 20 - 30\%$, and both are significantly larger than the gas mass M_{gas} (see Table 1). The radial profiles of the masses are shown for all clusters in Appendix A.

In order to calculate the baryonic mass we approximate the stellar contribution by $M_* = 0.15M_{gas}$, as is done in Pointecouteau & Silk (2005). We therefore estimate the total baryonic mass as $M_{baryon} = M_{gas} + M_*$. We find that the average $f_{gas}(r_{2500})$ for MOND is $14.2 \pm 0.2\%$, and that the average $f_{baryon}(r_{2500})$ is $16.4 \pm 0.2\%$ (Table 2). These results agree with the results obtained by Pointecouteau & Silk (2005), which report a value of $f_{baryon} = 20.2 \pm 2.0\%$ at a larger radius of r_{1000} . We find that, even with the inclusion of M_* , the baryon mass is still significantly lower than the total MOND mass for every cluster, confirming the fact that MOND is incapable of eliminating the need for dark matter in clusters. The mean f_{gas} and f_{baryon} in Table 2 are calculated as the weighted mean of all measurement, in which the weight is the standard error of each measurement. We also calculate the un-weighted means and their root-mean-square errors as $f_{gas} = 0.109 \pm 0.003$ (Newton) and $f_{gas} = 0.139 \pm 0.004$ (MOND), and $f_{baryon} = 0.125 \pm 0.004$ (Newton) and $f_{baryon} = 0.160 \pm 0.005$ (MOND).

We show the average distributions of f_{baryon} and M_{total}/M_{MOND} as function of physical radius in Figure 1. The distribution of f_{baryon} shows that the dynamical mass is always significantly higher than the baryonic mass. The distribution of M_{total}/M_{MOND} shows that the difference between the Newtonian and MOND masses are largest near the cluster core and at the largest radii, where the gravitational accelerations are lowest and therefore the MOND correction largest. Typical values of r_{2500} are between 0.5 and 1 Mpc, therefore we do not extrapolate these plots beyond 1 Mpc. The *Chandra* data presented in this paper were fit with a 100 kpc core cut (LaRoque et al., 2006), and therefore we do not extrapolate our models below this radius either.

The cluster baryon fraction calculated via the standard Newtonian dynamics in this paper ($\langle f_{baryon} \rangle = 0.1305$) and by other authors (e.g., McCarthy et al., 2007, for a review) are systematically lower than the WMAP

Table 1: Cluster Parameters And Masses For The Isothermal β -Model

Cluster	z	r_{2500} (arcsec)	D_A (Gpc)	M_{gas} ($10^{13}M_{\odot}$)	M_{total} ($10^{14}M_{\odot}$)	M_{Mond} ($10^{14}M_{\odot}$)
Abell1413	0.143	201.6 ^{+5.2} _{-4.6}	0.52	2.63 ^{+0.11} _{-0.1}	2.15 ^{+0.17} _{-0.14}	1.51 ^{+0.14} _{-0.12}
Abell1689	0.18	217.1 ^{+5.1} _{-5.5}	0.63	5.1 ^{+0.17} _{-0.17}	4.95 ^{+0.36} _{-0.36}	3.97 ^{+0.32} _{-0.33}
Abell1835	0.25	171.1 ⁺⁵ _{-4.4}	0.81	5.81 ^{+0.23} _{-0.2}	5.55 ^{+0.5} _{-0.42}	4.59 ^{+0.46} _{-0.38}
Abell1914	0.17	226.7 ^{+4.6} ₋₄	0.6	4.87 ^{+0.12} _{-0.1}	4.82 ^{+0.3} _{-0.25}	3.85 ^{+0.27} _{-0.22}
Abell1995	0.32	133.4 ^{+4.5} _{-4.7}	0.96	3.51 ^{+0.14} _{-0.14}	4.74 ^{+0.5} _{-0.48}	3.91 ^{+0.46} _{-0.44}
Abell2111	0.23	140.5 ^{+9.8} _{-8.9}	0.76	2.19 ^{+0.27} _{-0.23}	2.49 ^{+0.56} _{-0.44}	1.84 ^{+0.48} _{-0.37}
Abell2163	0.2	206.7 ⁺³ _{-2.9}	0.68	8.08 ^{+0.21} _{-0.2}	5.49 ^{+0.24} _{-0.23}	4.47 ^{+0.22} _{-0.21}
Abell2204	0.15	256.1 ⁺¹³ ₋₁₁	0.54	4.74 ^{+0.27} _{-0.24}	4.96 ^{+0.8} _{-0.64}	3.95 ^{+0.72} _{-0.57}
Abell2218	0.18	190 ^{+5.7} _{-5.4}	0.63	3.02 ^{+0.13} _{-0.12}	3.32 ^{+0.31} _{-0.27}	2.53 ^{+0.27} _{-0.24}
Abell2259	0.16	172.1 ^{+8.3} _{-7.9}	0.57	1.82 ^{+0.14} _{-0.14}	1.79 ^{+0.27} _{-0.24}	1.23 ^{+0.22} _{-0.19}
Abell2261	0.22	148.3 ^{+6.7} _{-6.3}	0.73	3.03 ^{+0.2} _{-0.19}	2.56 ^{+0.36} _{-0.31}	1.9 ^{+0.31} _{-0.26}
Abell267	0.23	131.3 ^{+8.5} _{-7.5}	0.76	2.24 ^{+0.2} _{-0.18}	2.03 ^{+0.42} _{-0.33}	1.46 ^{+0.35} _{-0.27}
Abell370	0.38	97.95 ^{+4.1} _{-4.1}	1.07	2.78 ^{+0.21} _{-0.2}	2.78 ^{+0.37} _{-0.33}	2.19 ^{+0.33} _{-0.29}
Abell586	0.17	181.6 ⁺⁸ ₋₇	0.6	2.27 ^{+0.13} _{-0.11}	2.48 ^{+0.34} _{-0.28}	1.8 ^{+0.29} _{-0.23}
Abell611	0.29	110.3 ^{+3.6} _{-3.5}	0.9	2.37 ^{+0.11} _{-0.11}	2.13 ^{+0.22} _{-0.2}	1.58 ^{+0.19} _{-0.17}
Abell665	0.18	160.5 ^{+3.6} _{-3.3}	0.63	2.63 ^{+0.1} _{-0.095}	2 ^{+0.14} _{-0.12}	1.41 ^{+0.11} _{-0.099}
Abell68	0.26	153 ⁺¹⁰ _{-9.3}	0.83	3.65 ^{+0.34} _{-0.31}	4.32 ^{+0.91} _{-0.74}	3.48 ^{+0.82} _{-0.66}
Abell697	0.28	133.1 ⁺⁵ _{-4.9}	0.88	4.4 ^{+0.28} _{-0.26}	3.46 ^{+0.4} _{-0.37}	2.73 ^{+0.36} _{-0.32}
Abell773	0.22	148.9 ^{+5.6} _{-5.3}	0.73	2.74 ^{+0.17} _{-0.15}	2.59 ^{+0.3} _{-0.27}	1.93 ^{+0.26} _{-0.23}
CLJ0016+1609	0.54	79.85 ⁺³ ₋₃	1.31	4.38 ^{+0.29} _{-0.29}	3.33 ^{+0.39} _{-0.37}	2.8 ^{+0.36} _{-0.34}
CLJ1226+3332	0.89	66.02 ^{+7.4} _{-6.5}	1.6	3.89 ^{+0.51} _{-0.46}	5.21 ⁺² _{-1.4}	4.8 ^{+1.9} _{-1.3}
MACSJ0647.7+7015	0.58	91.94 ^{+6.2} _{-5.7}	1.36	4.91 ^{+0.47} _{-0.42}	5.97 ^{+1.3} _{-1.1}	5.31 ^{+1.2} ₋₁
MACSJ0744.8+3927	0.69	58.88 ^{+3.5} _{-3.2}	1.47	3.08 ^{+0.27} _{-0.25}	2.26 ^{+0.42} _{-0.35}	1.89 ^{+0.39} _{-0.32}
MACSJ1149.5+2223	0.54	70.64 ^{+3.9} _{-3.6}	1.31	3.09 ^{+0.34} _{-0.3}	2.31 ^{+0.4} _{-0.34}	1.86 ^{+0.37} _{-0.3}
MACSJ1311.0-0310.	0.49	73.92 ^{+7.6} _{-6.6}	1.25	2.12 ^{+0.25} _{-0.21}	2.17 ^{+0.74} _{-0.53}	1.71 ^{+0.66} _{-0.47}
MACSJ1423.8+2404	0.55	65.93 ^{+2.1} ₋₂	1.32	2.26 ^{+0.1} _{-0.096}	1.94 ^{+0.2} _{-0.18}	1.54 ^{+0.17} _{-0.16}
MACSJ2129.4-0741.	0.57	72.42 ^{+4.6} _{-4.1}	1.35	3.27 ^{+0.3} _{-0.26}	2.82 ^{+0.57} _{-0.45}	2.35 ^{+0.53} _{-0.41}
MACSJ2214.9-1359.	0.482	91.31 ^{+5.1} _{-4.9}	1.23	3.94 ^{+0.32} _{-0.31}	3.85 ^{+0.68} _{-0.59}	3.24 ^{+0.63} _{-0.54}
MACSJ2228.5+2036	0.41	83.61 ^{+4.1} _{-3.8}	1.12	2.78 ^{+0.23} _{-0.21}	2.05 ^{+0.32} _{-0.27}	1.57 ^{+0.28} _{-0.23}
MS0451.6-0305	0.55	82.18 ^{+3.7} _{-3.5}	1.32	4.8 ^{+0.32} _{-0.3}	3.76 ^{+0.53} _{-0.46}	3.2 ^{+0.49} _{-0.43}
MS1054.5-0321	0.83	33.74 ^{+7.1} _{-8.5}	1.57	0.905 ^{+0.55} _{-0.49}	0.612 ^{+0.47} _{-0.36}	0.454 ^{+0.41} _{-0.29}
MS1137.5+6625	0.78	41.63 ^{+3.3} _{-2.9}	1.54	1.26 ^{+0.15} _{-0.14}	1.02 ^{+0.26} _{-0.2}	0.802 ^{+0.23} _{-0.18}
MS1358.4+6245	0.33	113.4 ^{+5.8} _{-5.2}	0.98	2.53 ^{+0.19} _{-0.17}	3.13 ^{+0.51} _{-0.41}	2.47 ^{+0.45} _{-0.36}
MS2053.7-0449	0.58	54.2 ^{+5.1} _{-4.6}	1.36	0.933 ^{+0.13} _{-0.12}	1.22 ^{+0.38} _{-0.29}	0.921 ^{+0.33} _{-0.24}
RXJ1347.5-1145	0.45	122.3 ^{+3.8} _{-3.6}	1.19	8.86 ^{+0.37} _{-0.35}	8.08 ^{+0.77} _{-0.69}	7.18 ^{+0.73} _{-0.65}
RXJ1716.4+6708...	0.81	45.01 ^{+4.4} _{-3.9}	1.56	1.23 ^{+0.19} _{-0.16}	1.39 ^{+0.45} _{-0.33}	1.14 ^{+0.41} _{-0.3}
RXJ2129.7+0005...	0.24	128.5 ^{+5.3} _{-4.9}	0.78	2.57 ^{+0.16} _{-0.14}	2.08 ^{+0.27} _{-0.23}	1.5 ^{+0.22} _{-0.19}
ZW3146.....	0.29	131.5 ^{+2.6} _{-2.5}	0.9	4.44 ^{+0.11} _{-0.11}	3.62 ^{+0.22} _{-0.2}	2.87 ^{+0.19} _{-0.18}

Table 2: Newtonian And MOND Mass Fractions

Cluster	$f_{\{gas\}}$		$f_{\{baryon\}}$	
	Newton	MOND	Newton	MOND
Abell1413	0.123 ^{+0.0041} _{-0.0045}	0.175 ^{+0.008} _{-0.0085}	0.141 ^{+0.0048} _{-0.0052}	0.201 ^{+0.0092} _{-0.0098}
Abell1689	0.103 ^{+0.0045} _{-0.0041}	0.129 ^{+0.0068} _{-0.0061}	0.118 ^{+0.0051} _{-0.0047}	0.148 ^{+0.0078} _{-0.007}
Abell1835	0.105 ^{+0.0047} _{-0.005}	0.127 ^{+0.0068} _{-0.0071}	0.12 ^{+0.0054} _{-0.0057}	0.146 ^{+0.0078} _{-0.0082}
Abell1914	0.101 ^{+0.0034} _{-0.0037}	0.127 ^{+0.0051} _{-0.0055}	0.116 ^{+0.0039} _{-0.0042}	0.146 ^{+0.0058} _{-0.0063}
Abell1995	0.0741 ^{+0.0051} _{-0.0046}	0.0897 ^{+0.0073} _{-0.0064}	0.0852 ^{+0.0059} _{-0.0053}	0.103 ^{+0.0084} _{-0.0074}
Abell2111	0.0883 ^{+0.0078} _{-0.0077}	0.119 ^{+0.014} _{-0.014}	0.101 ^{+0.009} _{-0.0088}	0.137 ^{+0.017} _{-0.016}
Abell2163	0.147 ^{+0.0026} _{-0.0025}	0.18 ^{+0.004} _{-0.004}	0.169 ^{+0.003} _{-0.0029}	0.208 ^{+0.0047} _{-0.0046}
Abell2204	0.0957 ^{+0.0094} _{-0.0099}	0.12 ^{+0.011} _{-0.014}	0.11 ^{+0.011} _{-0.011}	0.138 ^{+0.016} _{-0.016}
Abell2218	0.0909 ^{+0.0042} _{-0.0044}	0.119 ^{+0.0071} _{-0.0071}	0.105 ^{+0.0049} _{-0.005}	0.137 ^{+0.0081} _{-0.0082}
Abell2259	0.102 ^{+0.0069} _{-0.0069}	0.148 ^{+0.014} _{-0.013}	0.117 ^{+0.0079} _{-0.008}	0.17 ^{+0.016} _{-0.015}
Abell2261	0.118 ^{+0.0084} _{-0.0082}	0.159 ^{+0.015} _{-0.014}	0.136 ^{+0.0096} _{-0.0095}	0.183 ^{+0.017} _{-0.016}
Abell267	0.111 ^{+0.011} _{-0.011}	0.154 ^{+0.02} _{-0.019}	0.127 ^{+0.013} _{-0.013}	0.177 ^{+0.023} _{-0.022}
Abell370	0.1 ^{+0.0054} _{-0.0052}	0.127 ^{+0.009} _{-0.0084}	0.115 ^{+0.0062} _{-0.0059}	0.146 ^{+0.01} _{-0.0096}
Abell586	0.0916 ^{+0.0068} _{-0.0071}	0.126 ^{+0.012} _{-0.012}	0.105 ^{+0.0078} _{-0.0081}	0.145 ^{+0.014} _{-0.014}
Abell611	0.111 ^{+0.0058} _{-0.0057}	0.15 ^{+0.01} _{-0.0097}	0.128 ^{+0.0067} _{-0.0066}	0.173 ^{+0.012} _{-0.011}
Abell665	0.131 ^{+0.0036} _{-0.0038}	0.187 ^{+0.0072} _{-0.0074}	0.151 ^{+0.0042} _{-0.0044}	0.215 ^{+0.0083} _{-0.0085}
Abell68	0.0843 ^{+0.0089} _{-0.0083}	0.105 ^{+0.014} _{-0.012}	0.097 ^{+0.01} _{-0.0095}	0.12 ^{+0.016} _{-0.014}
Abell697	0.127 ^{+0.0066} _{-0.0063}	0.161 ^{+0.011} _{-0.01}	0.146 ^{+0.0076} _{-0.0073}	0.186 ^{+0.012} _{-0.012}
Abell773	0.106 ^{+0.0058} _{-0.0055}	0.142 ^{+0.01} _{-0.0095}	0.121 ^{+0.0067} _{-0.0063}	0.163 ^{+0.012} _{-0.011}
CLJ0016+1609	0.131 ^{+0.0067} _{-0.0063}	0.156 ^{+0.0099} _{-0.0091}	0.151 ^{+0.0078} _{-0.0073}	0.18 ^{+0.011} _{-0.01}
CLJ1226+3332	0.0746 ^{+0.015} _{-0.014}	0.081 ^{+0.018} _{-0.016}	0.0858 ^{+0.018} _{-0.016}	0.0931 ^{+0.021} _{-0.018}
MACSJ0647.7+7015	0.0821 ^{+0.0091} _{-0.0084}	0.0925 ^{+0.012} _{-0.011}	0.0945 ^{+0.011} _{-0.0097}	0.106 ^{+0.014} _{-0.012}
MACSJ0744.8+3927	0.136 ^{+0.012} _{-0.012}	0.163 ^{+0.018} _{-0.016}	0.157 ^{+0.014} _{-0.013}	0.187 ^{+0.02} _{-0.019}
MACSJ1149.5+2223	0.134 ^{+0.0077} _{-0.0078}	0.166 ^{+0.013} _{-0.013}	0.154 ^{+0.0088} _{-0.009}	0.191 ^{+0.015} _{-0.014}
MACSJ1311.0-0310.	0.0979 ^{+0.019} _{-0.017}	0.124 ^{+0.03} _{-0.025}	0.113 ^{+0.022} _{-0.019}	0.142 ^{+0.035} _{-0.028}
MACSJ1423.8+2404	0.116 ^{+0.0064} _{-0.0061}	0.147 ^{+0.0098} _{-0.0093}	0.134 ^{+0.0073} _{-0.007}	0.168 ^{+0.011} _{-0.011}
MACSJ2129.4-0741.	0.116 ^{+0.011} _{-0.011}	0.14 ^{+0.016} _{-0.016}	0.134 ^{+0.013} _{-0.013}	0.161 ^{+0.019} _{-0.018}
MACSJ2214.9-1359.	0.102 ^{+0.0088} _{-0.0084}	0.122 ^{+0.013} _{-0.012}	0.118 ^{+0.01} _{-0.0096}	0.14 ^{+0.015} _{-0.013}
MACSJ2228.5+2036	0.135 ^{+0.0087} _{-0.0087}	0.177 ^{+0.015} _{-0.014}	0.155 ^{+0.01} _{-0.01}	0.203 ^{+0.018} _{-0.017}
MS0451.6-0305	0.127 ^{+0.0088} _{-0.0085}	0.15 ^{+0.012} _{-0.012}	0.147 ^{+0.01} _{-0.0098}	0.172 ^{+0.014} _{-0.013}
MS1054.5-0321	0.145 ^{+0.015} _{-0.012}	0.191 ^{+0.051} _{-0.027}	0.166 ^{+0.018} _{-0.014}	0.219 ^{+0.059} _{-0.031}
MS1137.5+6625	0.123 ^{+0.015} _{-0.014}	0.157 ^{+0.024} _{-0.022}	0.141 ^{+0.017} _{-0.016}	0.18 ^{+0.028} _{-0.025}
MS1358.4+6245	0.0809 ^{+0.0061} _{-0.006}	0.102 ^{+0.0097} _{-0.0093}	0.093 ^{+0.007} _{-0.0069}	0.118 ^{+0.011} _{-0.011}
MS2053.7-0449	0.0761 ^{+0.012} _{-0.011}	0.101 ^{+0.02} _{-0.017}	0.0875 ^{+0.013} _{-0.012}	0.116 ^{+0.023} _{-0.02}
RXJ1347.5-1145	0.11 ^{+0.0056} _{-0.0055}	0.123 ^{+0.0071} _{-0.0069}	0.126 ^{+0.0065} _{-0.0063}	0.142 ^{+0.0082} _{-0.008}
RXJ1716.4+6708	0.0883 ^{+0.013} _{-0.011}	0.108 ^{+0.019} _{-0.016}	0.102 ^{+0.014} _{-0.013}	0.124 ^{+0.022} _{-0.019}
RXJ2129.7+0005	0.124 ^{+0.0088} _{-0.0077}	0.171 ^{+0.015} _{-0.014}	0.142 ^{+0.0094} _{-0.0088}	0.197 ^{+0.017} _{-0.016}
ZW3146	0.123 ^{+0.0044} _{-0.0043}	0.154 ^{+0.0066} _{-0.0064}	0.141 ^{+0.005} _{-0.0049}	0.178 ^{+0.0076} _{-0.0073}
Weighted Mean	0.114 ± 0.001	0.142 ± 0.002	0.131 ± 0.001	0.164 ± 0.002

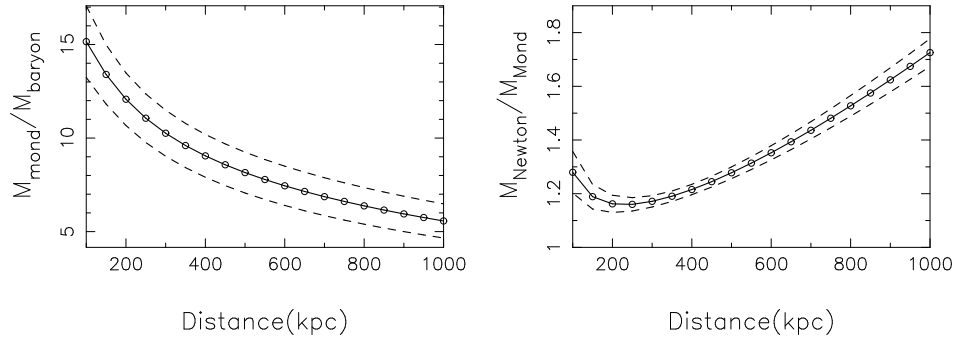


Figure 1: Average distribution of f_{baryon} and M_{total}/M_{MOND} for the 38 clusters; the dashed lines represent the root-mean-square uncertainty of the 38 measurements at each radius

value of $\Omega_B/\Omega_M=0.176\pm 0.02$ (Bennett et al., 2003), indicating the presence of undetected baryons in clusters. Within MOND, the results of this paper ($\langle f_{baryon} \rangle = 0.164$) and those of Pointecouteau & Silk (2005) are in statistical agreement with the WMAP value of Ω_B/Ω_M . We therefore speculate that MOND can in principle reconcile the cluster baryon fraction with the cosmic value of Ω_B/Ω_M , without the need for additional undetected baryons in clusters.

4.2. Results for a variable value of the MOND critical acceleration

We also consider the possibility of a_0 being a free parameter of the MOND theory, and use our data to determine it. To this end, we begin with Equation (13) for the MOND total mass, and calculate the value of the critical acceleration at each radius such that $M_{MOND}(r) = M_{baryon}(r)$,

$$M_{baryon}(r) = M_{MOND}(r) = \frac{M_{Newton}(r)}{\sqrt{1 + \left(\frac{a_\circ \mu m_p r_c^2 + r^2}{3\beta KT} \right)^2}}. \quad (14)$$

We then solve equation (14) for a_\circ and find that

$$a_\circ(r) = \frac{3\beta KT}{\mu m_p} \frac{r}{r_c^2 + r^2} \sqrt{\frac{M_{Newton}^2}{M_{baryon}^2} - 1}, \quad (15)$$

where M_{Newton} is given by equation (6). The radial distribution of a_o is shown for all clusters in Appendix B.

In Figure 2 we show the value of the critical acceleration calculated at r_{2500} for all 38 clusters, with a mean value of $a_o = 1.49 \pm 0.09 \times 10^{-7} \text{ cm/s}^2$. The main result is that the value of the "free" a_o at r_{2500} differs from that measured from galaxy rotation curves (e.g., Scarpa, 2006) by one order of magnitude. Moreover, we find statistically significant differences in the measurement of a_o at different radii for a given cluster (see Appendix B), and for different clusters at the same radius of r_{2500} (Figure 2).

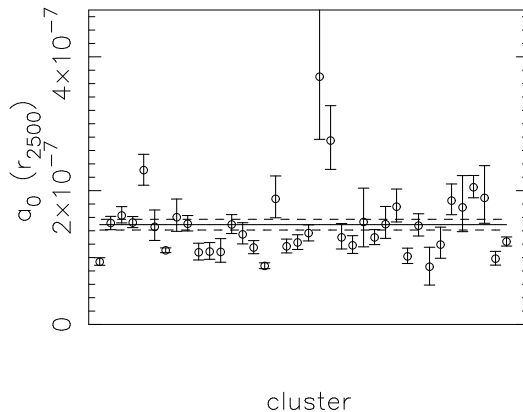


Figure 2: Calculation of $a_o(r_{2500})$. The horizontal line is the mean of a_o and its root-mean-square error, calculated as the un-weighted mean of the 38 measurements. The weighted mean of the 38 measurements is $a_o = 1.17 \pm 0.02 \times 10^{-7} \text{ cm/s}^2$.

We also show the average values of the best-fit critical acceleration a_o for the entire sample, as function of radius, in Figure 3. At all radii, the critical acceleration required to explain the hydrostatic MOND mass is at least one order of magnitude larger than the canonical value obtained from galaxy rotation curves (e.g., Scarpa, 2006).

5. Conclusions

In this paper we have measured gravitational and gas masses at r_{2500} for a sample of 38 high-redshift galaxy clusters using standard Newtonian gravity and Modified Newtonian Dynamics. This is the largest sample of galaxy clusters to which the MOND theory of gravity is applied to date.

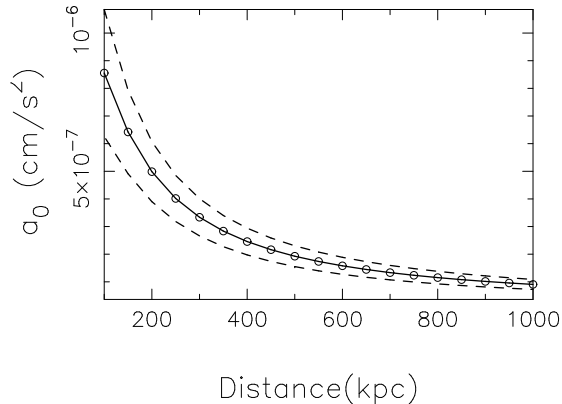


Figure 3: Average distribution of a_o for the 38 clusters; the dashed lines represent the root-mean-square uncertainty of the 38 measurements at each radius

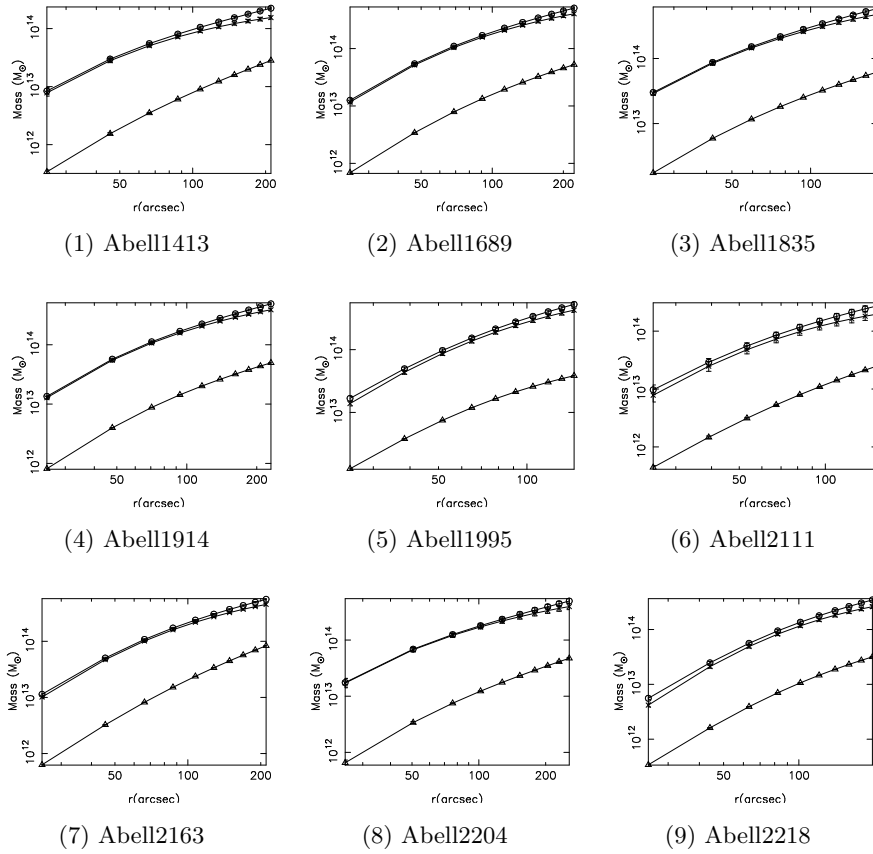
We initially used a fixed value of the MOND critical acceleration $a_o = 1.17e^{-8} cm/s^2$ and measured an average $\langle f_{baryon} \rangle = 0.164$; this result confirms that MOND does not eliminate the need for dark matter in galaxy clusters. Our work therefore confirms the previous reports by Angus et al. (2008) and Pointecouteau & Silk (2005). Further evidence that the MOND theory of gravity is unable to explain X-ray observations of galaxy clusters is found by a fit of our X-ray data to a MOND model with varying a_o . The value of a_o required to achieve a baryon fraction of unity varies both with cluster radius, and between clusters; moreover, the mean value of this free a_o is one order of magnitude larger than that required by galaxy dynamics. We therefore conclude that X-ray observations of the hot cluster plasma do require strong presence of dark matter even when MOND is used.

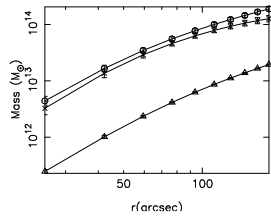
This analysis also finds that the f_{baryon} at r_{2500} calculated using MOND is in statistical agreement with the WMAP value of Ω_b/Ω_M , similar to the results of Pointecouteau & Silk (2005).

Appendix A

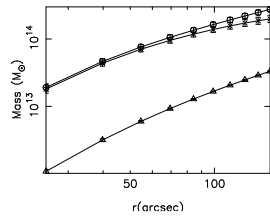
In this appendix we provide the radial profiles of the gas, Newtonian and MOND masses for all clusters, calculated between 100 kpc and r_{2500} .

Figure 4: Distribution of M_{gas} , M_{total} , and M_{MOND} as a function of radius(arcsec) for all 38 clusters. The symbols are used as follows: \circ for M_{total} , \times for M_{MOND} , and \triangle for M_{gas}

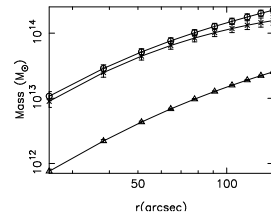




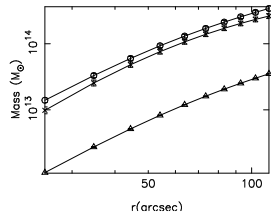
(10) Abell2259



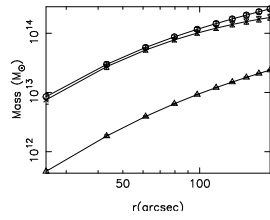
(11) Abell2261



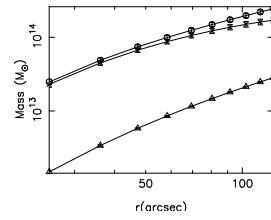
(12) Abell267



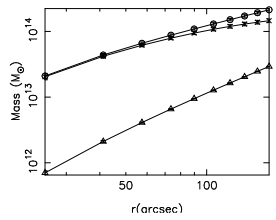
(13) Abell370



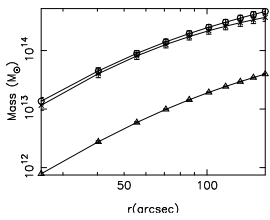
(14) Abell586



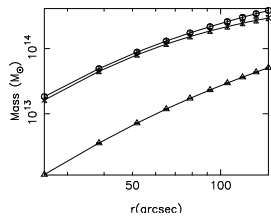
(15) Abell611



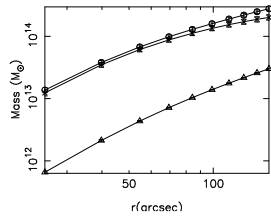
(16) Abell665



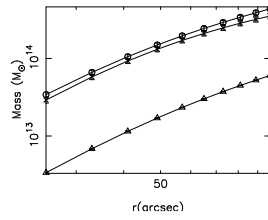
(17) Abell668



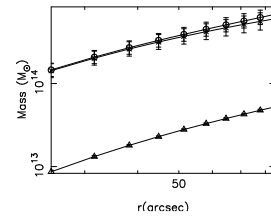
(18) Abell697



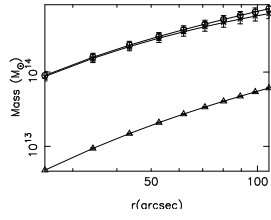
(19) Abell773



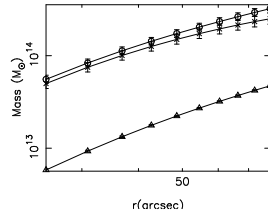
(20) CLJ0016+1609



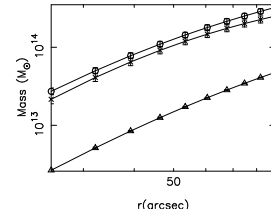
(21) CLJ1226+3332



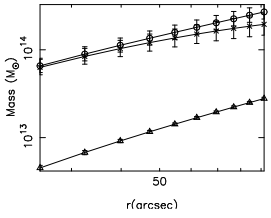
(22) MACSJ0647.7+7015



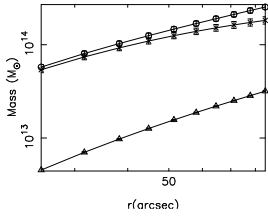
(23) MACSJ0744.8+3927



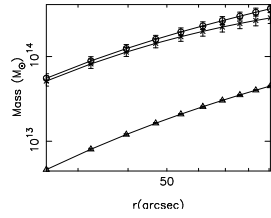
(24) MACSJ1149.5+2223



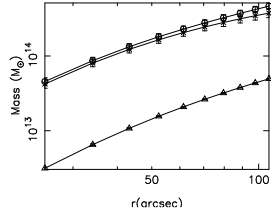
(25) MACSJ1311.0-0310



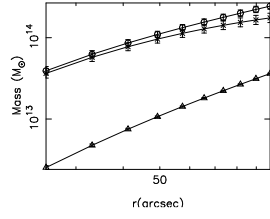
(26) MACSJ1423.8+2404



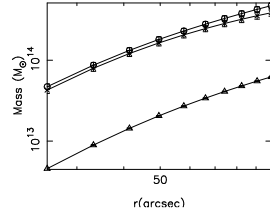
(27) MACSJ2129.4-0741



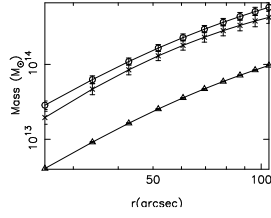
(28) MACSJ2214.9-1359



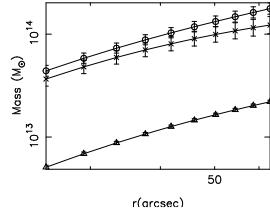
(29) MACSJ2228.5+2036



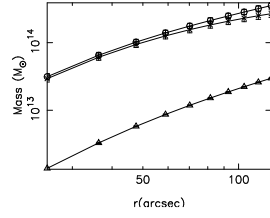
(30) MS0451.6-0305



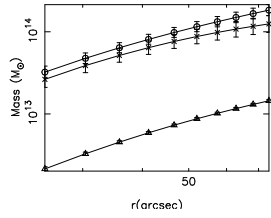
(31) MS1054.5-0321



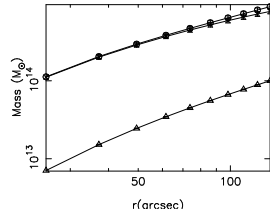
(32) MS1137.5+6625



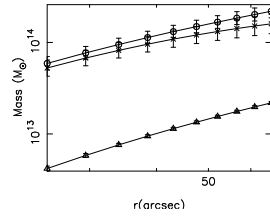
(33) MS1358.4+6245



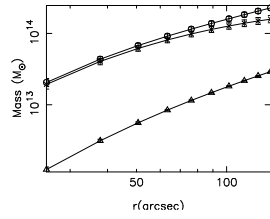
(34) MS2053.7-0449



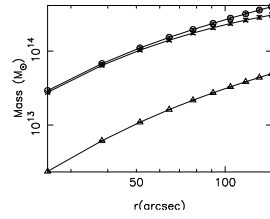
(35) RXJ1347.5-1145



(36) RXJ1716.4+6708



(37) RXJ2129.7+0005

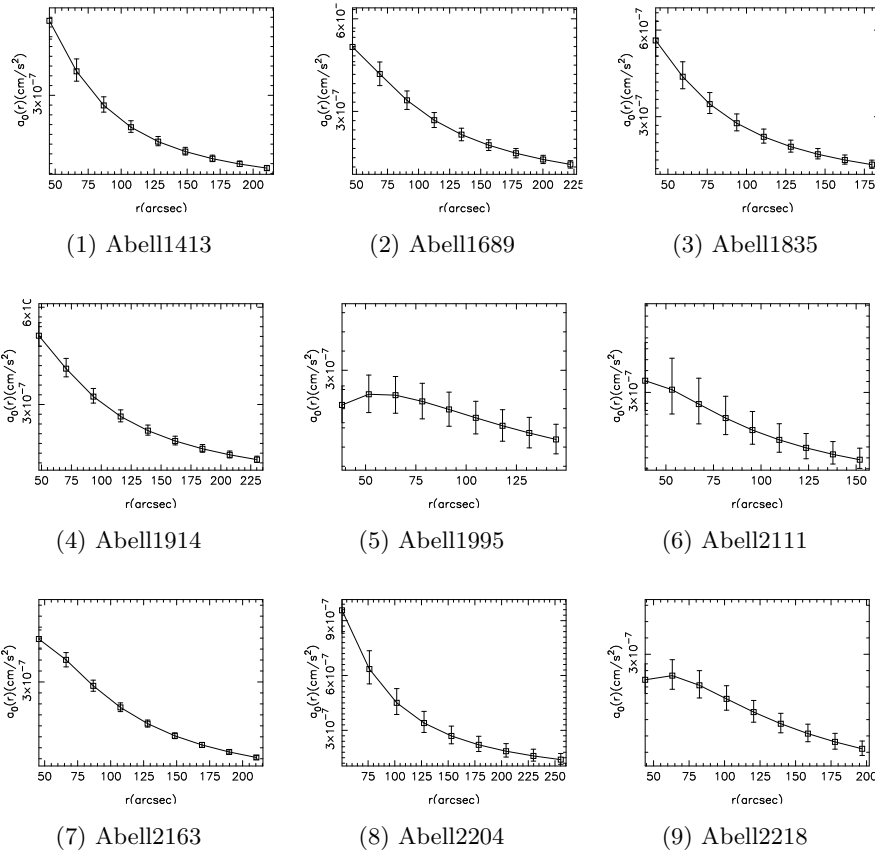


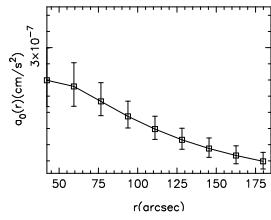
(38) ZW3146

Appendix B

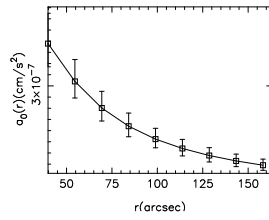
In this Appendix we provide the radial distribution of the best-fit values of the critical acceleration a_0 , for all clusters. The plot extend between 100 kpc and r_{2500} .

Figure 6: The critical acceleration a_0 as a function of radius, under the condition $M_{MOND} = M_{baryon}$ for all 38 clusters

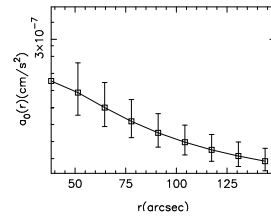




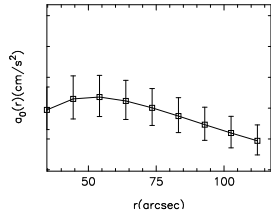
(10) Abell2259



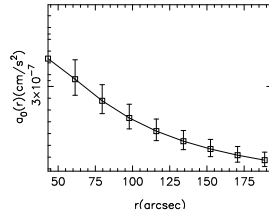
(11) Abell2261



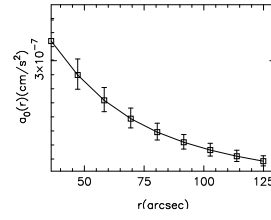
(12) Abell267



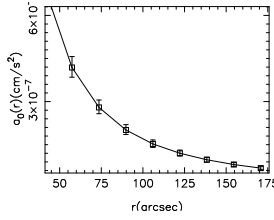
(13) Abell370



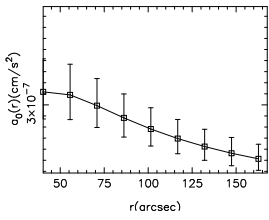
(14) Abell586



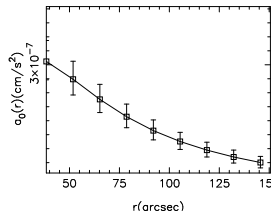
(15) Abell611



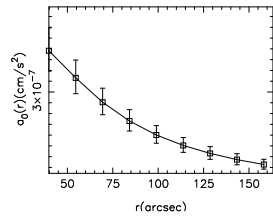
(16) Abell665



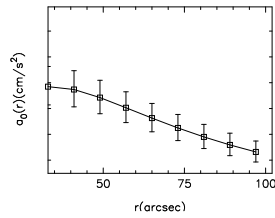
(17) Abell68



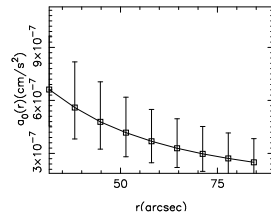
(18) Abell697



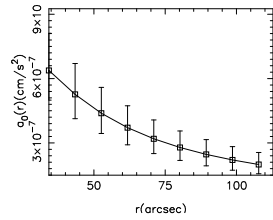
(19) Abell773



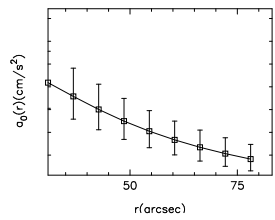
(20) CLJ0016+1609



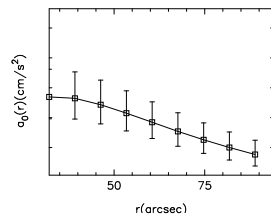
(21) CLJ1226+3332



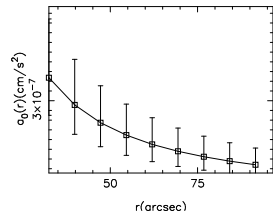
(22) MACSJ0647.7+7015



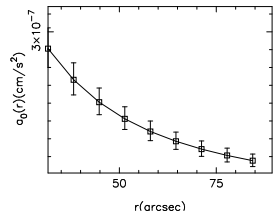
(23) MACSJ0744.8+3927



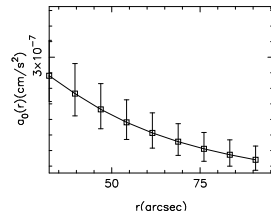
(24) MACSJ1149.5+2223



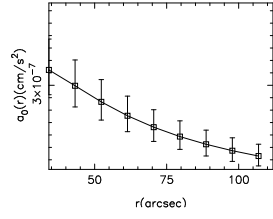
(25) MACSJ1311.0-0310



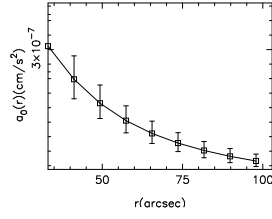
(26) MACSJ1423.8+2404



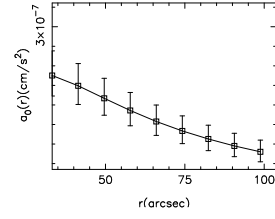
(27) MACSJ2129.4-0741



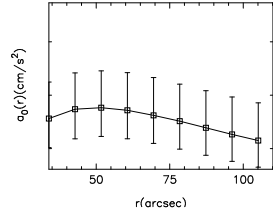
(28) MACSJ2214.9-1359



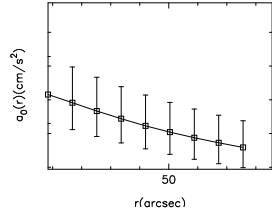
(29) MACSJ2228.5+2036



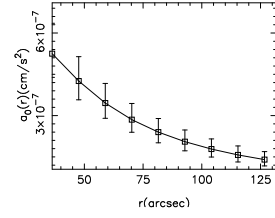
(30) MS0451.6-0305



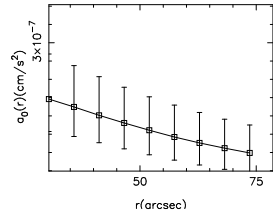
(31) MS1054.5-0321



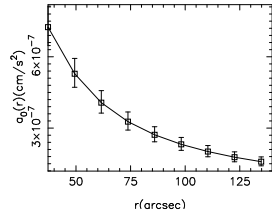
(32) MS1137.5+6625



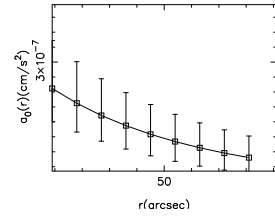
(33) MS1358.4+6245



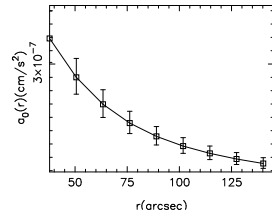
(34) MS2053.7-0449



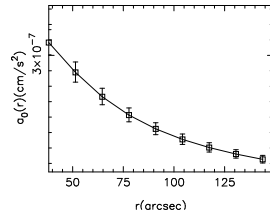
(35) RXJ1347.5-1145



(36) RXJ1716.4+6708



(37) RXJ2129.7+0005



(38) ZW3146

References

- Aguirre, A., Schaye, J., & Quataert, E. 2001, *Astrophysical Journal*, 561, 550
- Angus, G. W., Famaey, B., & Buote, D. A. 2008, *Mon. Not. Royal Astronomical Soc.*, 676
- Bennett, C. L. et al. 2003, *Astrophysical Journal Supplement*, 148, 1
- Birkinshaw, M., Hughes, J. P., & Arnaud, K. A. 1991, *Astrophysical Journal*, 379, 466
- Bonamente, M., Joy, M., LaRoque, S. J., Carlstrom, J. E., Nagai, D., & Marrone, D. P. 2008, *Astrophysical Journal*, 675, 106
- Bonamente, M., Joy, M. K., Carlstrom, J. E., Reese, E. D., & LaRoque, S. J. 2004, *Astrophysical Journal*, 614, 56
- Bonamente, M., Joy, M. K., LaRoque, S. J., Carlstrom, J. E., Reese, E. D., & Dawson, K. S. 2006, *Astrophysical Journal*, 647, 25
- Carroll, S. M., Press, W. H., & Turner, E. L. 1992, *Annual Rev. Astron. Astroph.*, 30, 499
- Cavaliere, A., & Fusco-Femiano, R. 1976, *Astronomy and Astrophysics*, 49, 137
- . 1978, *Astronomy and Astrophysics*, 70, 677
- LaRoque, S. J., Bonamente, M., Carlstrom, J. E., Joy, M. K., Nagai, D., Reese, E. D., & Dawson, K. S. 2006, *Astrophysical Journal*, 652, 917
- McCarthy, I. G., Bower, R. G., & Balogh, M. L. 2007, *Mon. Not. Royal Astronomical Soc.*, 377, 1457
- Milgrom, M. 1983, *Astrophysical Journal*, 270, 365
- Pointecouteau, E., & Silk, J. 2005, *Mon. Not. Royal Astronomical Soc.*, 364, 654
- Sanders, R. H. 1999, *Astrophysical Journal Lett.*, 512, L23
- Scarpa, R. 2006, in *American Institute of Physics Conference Series*, Vol. 822, *First Crisis in Cosmology Conference*, ed. E. J. Lerner & J. B. Almeida, 253–265